Materials Today Communications 30 (2022) 103023

Contents lists available at ScienceDirect

Materials Today Communications

journal homepage: www.elsevier.com/locate/mtcomm

Geometrical control of degradation and cell delivery in 3D printed nanocellulose hydrogels

Rupambika Das [a], Cheng Pau Lee [a], Anupama Prakash [b], Michinao Hashimoto [a], Javier G. Fernandez [a,*]

[a] Singapore University of Technology and Design, 8 Somapah Road, 487372 Singapore, Singapore
[b] National University of Singapore, 21 Lower Kent Ridge Rd, 119077 Singapore, Singapore

ARTICLE INFO

Keywords:
3D bioprinting
Nanocellulose
Cell encapsulation
Geometrical design
Enzymatic degradation

ABSTRACT

Hydrogels based on cellulose nanofibers are rapidly gaining attention in biomedical applications due to their biocompatibility, exogenous degradation to mammals, and their unique properties and functionalities distinct from molecular cellulose and wood pulp. Among those properties, the mechanical toughness and shear thinning behavior make these hydrogels particularly well suited to be extruded and bioprinted. The recent discovery of their ability to support stem cell growth while preserving their pluripotency adds to their promising use as carriers for the storage and controlled delivery of stem cells. However, the simultaneous stemness preservation and biodegradation dependency on the degree of oxidation avoids their optimization by chemical modifications. Here, those limitations are circumvented by bioprinting nanocellulose hydrogels without additives, enabling geometry-controlled degradation and cell retrieval at a constant degree of oxidation. This approach is demonstrated by tuning cell delivery from hours to days in nanocellulose scaffolds—of both plant and bacterial origin—in similar compositions and volumes but different apparent areas. The results, which are generalizable to other biodegradable polymers, provide a new approach for the encapsulation, storage, and delivery of mammalian cells in cellulose hydrogel, with a direct application in stem cell biology, tissue engineering, and biomedical devices.

1. Introduction

Cellulose nanofibers (CNFs) are strong, stiff, highly crystalline fibers extracted from the raw cellulose of plants or bacteria that exhibit mechanical and chemical properties different from those of the raw cellulose they are extracted from and the separate cellulose molecules making them [1]. Among those unique properties, cell-laden CNF hydrogels have recently gained attention because of their intrinsic ability to delay the differentiation of encapsulated stem cells, removing the need for exogenous inhibitory factors (e.g., Leukemia Inhibitory Factor) and positioning them as a promising carrier for stem cell delivery and preservation [2]. However, this distinctive functionality of CNF hydrogels conflicts with the chemical modifications and cross-linking employed for their formation into 3D scaffolds and the tweaking of their degradation and cell delivery profiles [3]. An alternative route to manage the degradability of CNF hydrogels while preserving their chemical characteristics and functionality would enable their general use as carriers of stem cells with controlled loading, preservation, and release of the cell population.

Due to their ubiquitous origin, CNFs are primarily considered to have the potential to become a sustainable structural material for manufacturing composites and coatings [4]. This promising application of nanocellulose in general manufacturing is still hindered by the ecological unsustainability of their extraction methods and high production costs [5,6], which have not prevented the rapid growth of its uses in hydrogel format in medical applications as a substrate and bioink closely mimicking extracellular matrix (ECM) structural characteristics [7]. CNF hydrogels are mixed with other hydrogels, chemically modified, and cross-linked to achieve acceptable levels of stability and shape fidelity of the three-dimensional cell-laden scaffolds formed with them [8]. These manufacturing strategies enable the generation of stable printed scaffolds, which are not possible when the materials are used independently or without modification, and have provided promising results for the use of adherent cells, thereby enabling the production of

* Corresponding author.
E-mail address: javier.fernandez@sutd.edu.sg (J. G. Fernandez).

https://doi.org/10.1016/j.mtcomm.2021.103023
Received 7 July 2021; Received in revised form 5 October 2021; Accepted 17 November 2021
Available online 24 November 2021

3D fibroblast cultures [8], liver mimetic constructions [9], and tissue mimicking [10].

The ability to encapsulate cells is neither novel nor unique to CNF hydrogels; however, the current elevated biomedical interest in these hydrogels results from the growing body of data reporting a delayed differentiation in stem cells cultured on nanocellulose surfaces and volumes [11,12]. The applicability of this intrinsic functionality of CNF hydrogels for preserving pluripotency was recently demonstrated with a sustained expression of octamer-binding transcription factor 4 (OCT-4) in populations of stem cells embedded in three-dimensional nanocellulose hydrogels [2]. This ability to maintain pluripotency and produce differentiation patterns similar to those in vivo is a very rare property, particularly for natural polymers, enabling the preservation, delivery, and controlled development of stem cells [13]. In the case of CNF hydrogels, the material's behavior is enhanced by their unique combination of the specific enzymatic degradation and exogenesis in mammals, making it suitable to be selectively degraded and enabling the controlled release and recovery of the intact mammalian cell load.

However, the pluripotency preservation and the control of the degradation/delivery are parameters that depend on the sterically available chemical groups on the surface of CNFs [14]. As a result, the traditional methods for tuning carrier degradation, performed through controlled chemical modifications and blending with other hydrogels, cannot be applied without affecting the hydrogel's functionality. To bypass this limitation, we demonstrate the dependency of the degradation of CNF scaffolds with their apparent area, and the use of this dependency for controlled degradability and cell delivery based on geometry, without modifying the chemistry of the encapsulation. This approach, enabled by the flexibility of current bioprinting techniques, is also a generalizable strategy for unlinking the chemical/functional aspects of hydrogel encapsulations (governing the cell-substrate interactions) and their degradability (controlling cell release and bioabsorption). This was achieved after the first optimization of CNF hydrogels for printing without cross-linking agents, based on their thixotropic characteristics, enabling their immediate hardening after being extruded through a high gauge needle, avoiding the need for exogenous hardening factors.

2. Results and discussion

The hydrogels were prepared by TEMPO free radical oxidation reaction, where the hydroxyl groups of the native cellulose were substituted by carboxylate ions (Fig. 1a). Bacteria and plant cellulose (Supplementary Fig. S1) were processed in parallel to study the generalization of the approach and the possible advantages of each one for different solutions. In general, plant cellulose is preferred in large-scale applications due to its ubiquity and simple production [15]. In contrast, bacteria cellulose has the advantage of higher degrees of crystallinity and less processing, as it is naturally produced without lignin, hemicellulose, or polysaccharides, which are common in plants [16–18]. The two sources of cellulose were processed to obtain a final working concentration of 1% (w/v) of TEMPO-oxidized bacterial cellulose (TOBC) and TEMPO-oxidized plant cellulose (TOPC) in water (Fig. 1b and Supplementary Fig. S1). The degree of oxidation was critically chosen within the narrow window where both the stem cell pluripotency preservation and suitability for enzymatic degradation coexist [2]. This decision was based on the hydrogel characteristics after incubation in cell media. The glucose in the cell culture medium demonstrated enhanced inter-chain interactions, which hampered and nullified the enzymatic degradation of the CNFs [19].

The raw cellulose's morphological characteristics at the microscale varied with the source, but the different materials homogenized into a similar substance after oxidation (Fig. 1b). The raw fibers—from plant origin—reduced their diameter from the original 1 μm to the range of 50–100 nm, similar to that of the raw bacterial cellulose fibers, which in contrast, did not see their morphology affected by the oxidation process. This effect has been related to the different degrees of crystallinity, as the oxidation process removes low crystalline cellulose, which is copious in plant cellulose but practically non-existent in bacterial cellulose [20]. The achievement of the right electrical surface characteristics for stemness preservation was corroborated by measuring the zeta potential (−3.81 mV for TOPC and −3.77 mV for TOBC, corresponding to 3.2 and 3.11 mmol/g carboxylate ions). The surface charge values matched previous reports, confirming the success of the protocol and the production of the CNFs with the intended characteristics [2,21]. The hydrogel's negative surface charge has been suggested to be responsible for inhibiting stem cell interaction with the surrounding matrix and promoting cell-to-cell interaction, resulting in an environment and differentiation pattern similar to those of in vivo embryogenesis [13,22,23].

Despite the similar morphology, the same oxidation process of cellulose from different sources results in hydrogels with slightly different

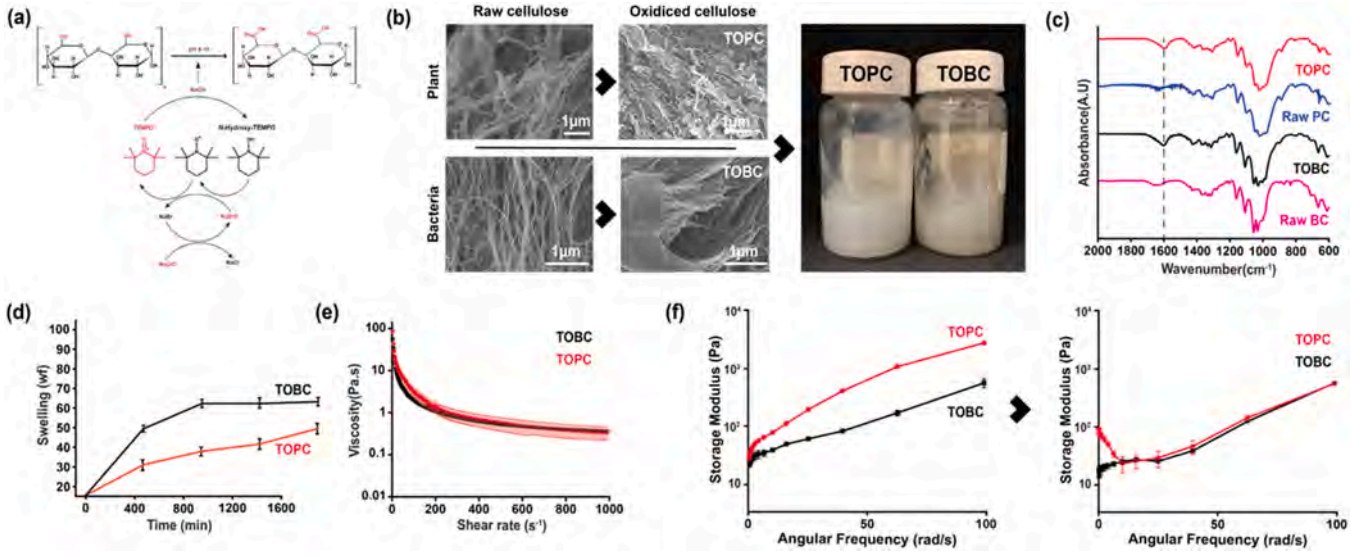

Fig. 1. Synthesis and morphological characteristics of TOBC and TOPC. (a) The biochemical pathway followed to formulate cellulose-derived hydrogels. (b) Scanning electron microscopy images of TOBC and TOPC. (c) Functionalization confirmation by FTIR. (d) Water absorption or swelling degree measurement as a function of time. (e) Viscosity measurement of the hydrogel systems. (f) storage modulus measurement of the hydrogels (left) and after (right) incubation in media.

characteristics. The infrared (i.e., FTIR) fingerprint of TOBC and TOPC and their comparison with the original raw materials confirmed the purity of the sources and the successful oxidation of both. This is observable in the new clear signals at ca. 1600 cm^{-1} due to the vibration of the carboxylate groups [24] (Fig. 1c). However, despite the similarities at molecular and supramolecular levels of the oxidized CNFs from different sources, TOBC shows a significantly higher water retention ability than TOPC (72 ± 24.4 g of water per g of CNF for TOBC and 57 ± 15 for TOPC; Fig. 1d). This difference is usually associated with varying degrees of substitution of –COOH during free radical oxidation when the CNFs are from the same source [25,26]. Here, the relatively low difference of surface charges can not explain the differences in water retention on their own, suggesting other differences at intermediate levels of the CNFs hierarchical organization.

The rheological differences resulting from the water content of gels from different sources of raw cellulose, while empirically significant, are negligible from the practical application point of view. The pressure ranging between 10 and 100 Pa made both the polymers suitable for printing free-standing structures without any requirement of cross-linking agents (Supplementary Fig. S2, Supplementary Videos 1-3). It is noteworthy that while the viscosity of CNF hydrogels is critical for this study, as it conditions the extrusion (Fig. 1e) and malleability of the hydrogels [27], these values should not be considered final from a biological perspective. The stiffness of the construct will increase after incubation in the media due to the physical cross-linking taking place as a result of the high glucose content in the cell culture medium [2]. In this case, the storage moduli, post-incubation, is still two orders of magnitude under the 10 Kpa, the commonly assumed threshold for supporting cell viability and migration [28](Fig. 1f).

The ability to print the CNF hydrogels without using an exogenous cross-linker and a composition suitable to preserve differentiation and enzymatic degradation enables the exploration of geometry to control the latter. The strategy to modify and maximize the apparent surface, via topography and porosity, is a common strategy for enhancing chemical reactions and is particularly critical in batteries, electrodes, and solid catalysts. Despite the central role of biodegradation in biomedical applications, its control nowadays is uniquely based on reagent concentrations and material composition.

To evaluate the use of the apparent area to tune the degradation of CNF hydrogels, we printed CNF hydrogels of the same weight and volume in a standard grid pattern, with infill densities of 12.5%, 18%, 25%, 50%, and 100% (Supplementary Fig. S3). The scaffolds were later incubated overnight in the culture medium to reach their final mechanical characteristics. The degradation by cellulase from *Trichoderma reesei* confirmed the hypothesis that, similar to most surface-dependent reactions and effects, the apparent area strongly dominates enzymatic hydrolysis [29]. Therefore, combined with a freeform manufacturing method, it can be used as a non-chemical approach to tune biodegradation. The constructs with infill density from 12.5% to 18% (Fig. 2a) degraded within five hours of incubation (first time point). This degradation time grew to 10, 15, and 26 h for the same volume of CNF hydrogels with infill densities of 25%, 50%, and 100%, respectively (Fig. 2b-e).

Cellulose fibers at levels of oxidation preserving their enzymatic susceptibility to degradation enable the avoidance of more aggressive and unspecific degradation methods, such as alkali digestion, and their use as carriers for cell delivery [30–32]. Two populations of mature cells (i.e., NIH-3T3 mouse fibroblasts) and stem cells (i.e., R1/E pluripotent mouse embryonic stem cells) were used for performing the biocompatibility assay. The viability of bioprinted cells, along with that of the control samples, was measured on days 1, 5, 7, and 10. The fibroblasts in TOBC and TOPC began to stretch and elongate within 24 h post-encapsulation in the unprinted material [33], a process that was delayed until day seven in the 3D printing scaffold of the same material (Fig. 3a, Supplementary Fig. S4). A similar delayed setting was observed in the case of embryonic stem cells, where the formation of embryoid bodies is apparent by day five in unprinted samples but is delayed until day 10 in the 3D printed scaffolds (Fig. 3b and Supplementary Fig. S5). One of the possible reasons for this phenomenon could be the stress experienced by the cells during extrusion.

Thixotropic hydrogels are generally accepted as ideal cell carriers in biomedical applications involving high shear stress, such as printing and injecting [34,35]. This is because the shear-thinning behavior of the gel facilitates extrusion, allowing for the use of relatively low pressures, and absorbs the energy of extrusion that would otherwise be transferred to the encapsulated cell population [36]. This protective behavior of the gel can be observed in the large cell viability post-extrusion; however, the stressful process's effect is observable in the delayed setting time for both cell types (Fig. 3c). Furthermore, this delayed setting is amplified by using complex geometries and gaps, marginalizing the cell

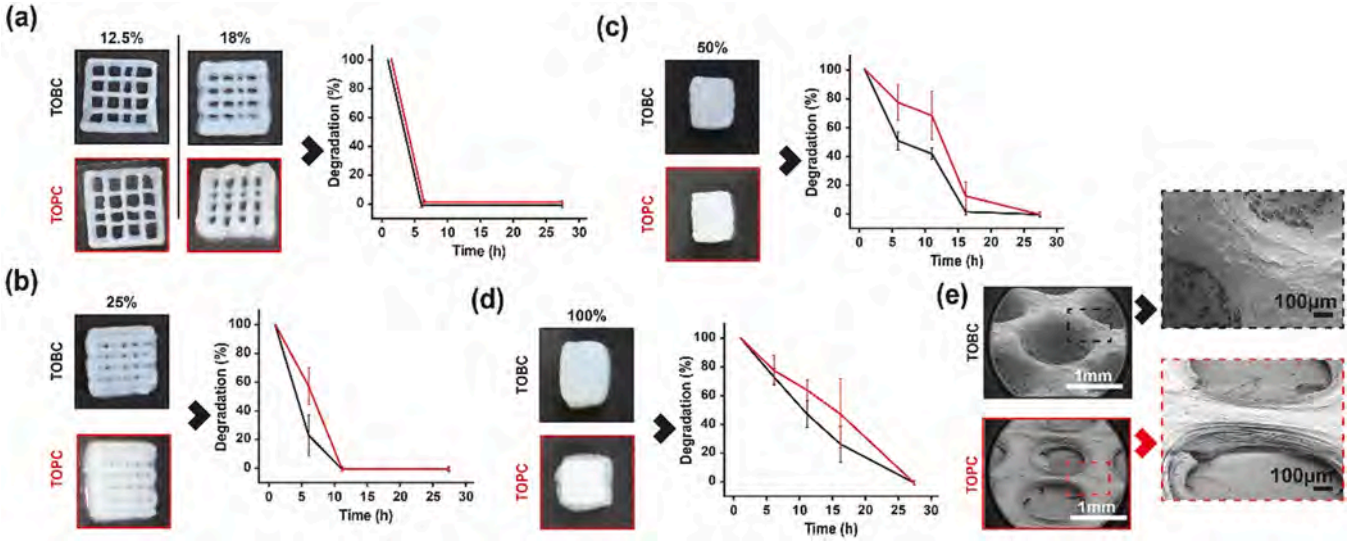

Fig. 2. Degradation profile of CNF hydrogels. (a) Examples of 3D printed scaffold with 12.5% and 18% infill density and its degradation by the cellulase enzyme. (b, c,d) Examples of 3D printed scaffold with 25%,50%, and 100% infill density (Supplementary Fig. S2). (e) Scanning electron microscopy images of the 3D printed scaffolds depicting structural stability (Images taken from the standard mesh structure to test printability with a spacing of about 2.7 mm). Error bars represent standard deviation in non-zero measurements and instrument error baseline measurements.

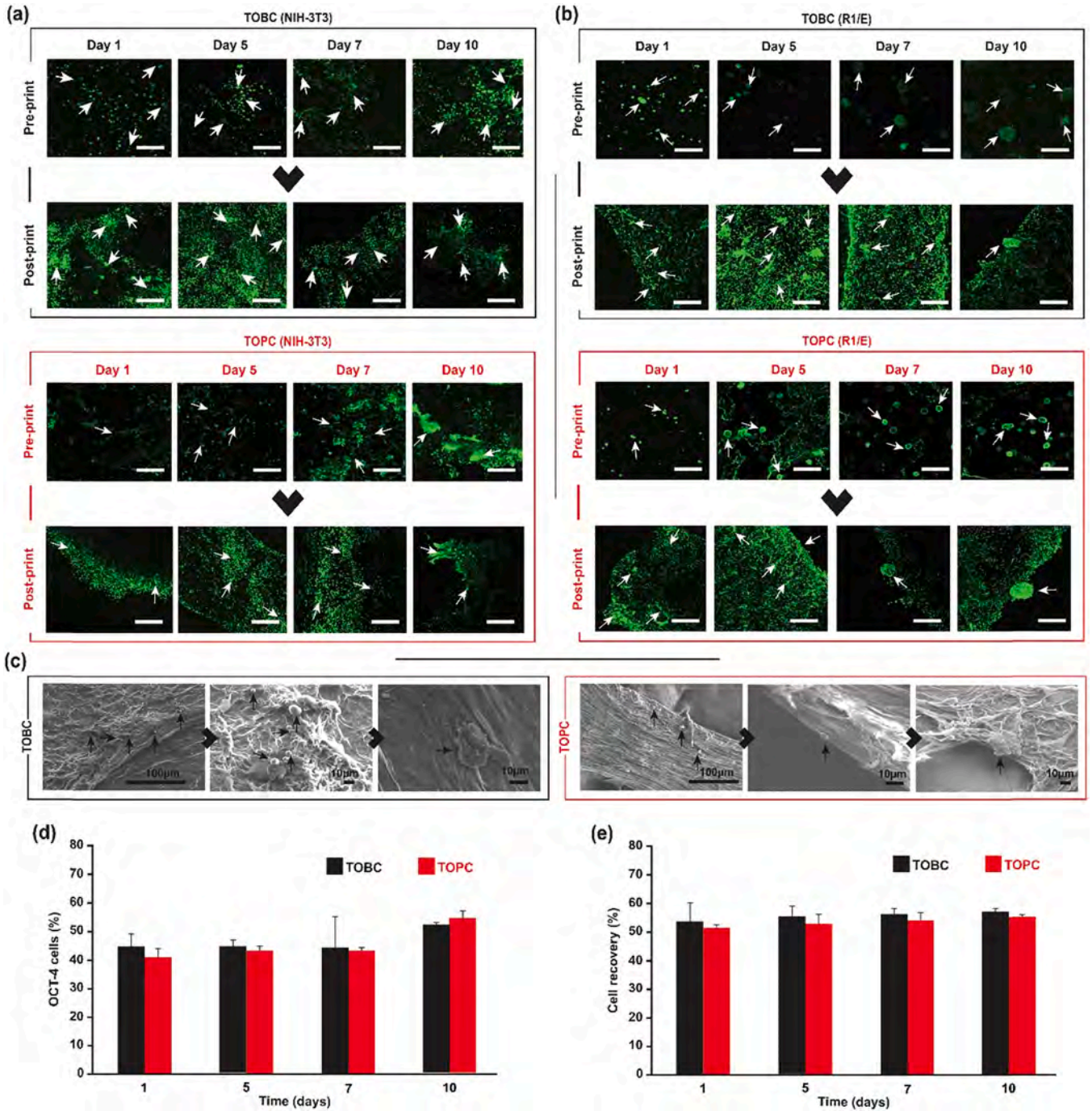

Fig. 3. 3D bioprinting of NIH-3T3 and R1/E encapsulated in TOPC and TOBC. (a and b) Cells encapsulated in TOBC and TOPC to monitor their growth pattern in both printed and non-printed culture conditions. (c) Scanning electron microscopy images of the 3D printed cells showing cell distribution and fiber alignment. (d) OCT-4 expression on days 1, 5, 7, and 10 was performed by flow cytometry (Supplementary Figs. S6, S7, and S10). (e) Total viable cells recovered at different time points. Amounts are relative to the number of cells added to the gel before printing. (Viability and pluripotency data are available in Supplementary Figs. S8, S9, S10, and S11).

population and reducing the number of close neighbor cells, resulting in the mentioned five-day delay in their setting [37].

The CNF encapsulation was enzymatically degraded on days 1, 5, 7, and 10, delivering the stored cell population. The harvested cells were analyzed for their pluripotency (Fig. 3d, Supplementary Figs. S6, S7, and S10), viability (Supplementary Figs. S8, S9, and S10), and efficiency of the extraction as a comparison of the number of cells encapsulated and recovered (Fig. 3e and Supplementary Fig. S10). The viability test confirmed the enzymes' highly selective action, enabling the cells' delivery without affecting their polysaccharide structures, which otherwise would result in necrosis [38,39]. Similarly, the OCT-4 levels measured after ten days post-encapsulation confirmed the pluripotency preservation on the 3D printed hydrogels and recapitulated previous results with the same CNF-based material [2].

3. Conclusion

In conclusion, we presented the formulation of CNF bioinks from two different sources (plants and bacteria) to enable the printing of scaffolds while maintaining their suitability for enzymatic degradation and

pluripotency preservation. The hydrogels from the two cellulose sources were compared for mechanical properties, biocompatibility, and printability. Despite the different purity and crystallinity between sources, there was a homogenization of the material post-oxidation to a hydrogel of similar mechanical, rheological, or biological characteristics. The use of geometry, specifically the specific area of the constructs, enabled the tuning of the degradation from a few hours to days without altering the material's chemistry, thereby preserving its biological characteristics. The delivered cells' viability was demonstrated, and simultaneously, previous results on pluripotency preservation were recapitulated. We believe these results present a novel use of bioprinting as a technique to tune the biodegradation of cell-laden biological scaffolds independent of cell-scaffold interactions. While this was demonstrated here for CNF hydrogels due to the uniqueness of their pluripotency preservation nature and immediate impact in the field, we believe this strategy can be generalized for other cell-laden biomedical solutions.

4. Materials and methods

4.1. TEMPO oxidized Plant CNF preparation (TOPC)

The cellulose slurry (3% wt.) which is derived from plants was obtained by a company in Canada called Cellulose Lab (Fredericton, NB, Canada). 17 g of the slurry was weighed which accounts for 0.5 g of dry weight of cellulose. The cellulose slurry was thoroughly dispersed in 50 ml of DI water before the oxidation reaction. The beaker with the starting volume was placed on a magnetic stirrer and reagents of oxidation were added one by one. TEMPO (8 mg,0.2 mmol) and NaBr (51.2 mg, 2 mmol) were added to the slurry followed by NaOCl solution (5% w/v,20 mmol) in a dropwise manner. pH was always maintained at 10.5 and was regulated by 0.5 M NaOH until no more variation was observed. The reaction was carried out at room temperature. After the reaction was completed the oxidized cellulose fibers were washed for a few times until the pH dropped to 7.4, which is recorded by a pH paper. The fibers were then homogenized using an ultrasonic probe homogenizer (Fisherbrand™ Model 505) to get a final concentration of 1% (w/v) CNF hydrogel.

4.2. Bacterial cellulose preparation

Bacterial cellulose was produced in-house by the fermentation of sweetened tea using a symbiotic culture of bacteria and yeast (SCOBY), popularly used to make Kombucha. SCOBY in starter culture tea was purchased from Kombucha tea enthusiasts in Singapore. Fresh culturing tea media was prepared by boiling 2.5 cups of water with half a cup of sugar and 1 black tea bag (Lipton). The SCOBY was placed in the fresh tea media once it reached room temperature along with the starter tea, and the container was sealed with a cloth to allow air exchange. Fermentation was carried out in a dark place for 1–2 weeks at 28℃ without shaking. A 1–2 mm pellicle of cellulose was obtained at the air-liquid interface after one week of culturing. Longer culturing times led to thicker pellicles.

4.3. TEMPO oxidized Bacterial CNF preparation (TOBC)

Newly formed bacterial cellulose pellicles were removed from the tea media and washed with water, followed by a quick wash in 70% ethanol. The sheets were then placed in boiling hot water and washed for 30 min on a magnetic stirrer. They were then cleaned in hot NaOH solution (0.1 M) for 20 min on a magnetic stirrer to remove the tea, followed by another wash in water to get rid of all the NaOH completely. The pellicles were then placed in − 80 ℃ until frozen, followed by freeze drying before hydrogel preparation.

The dried sheets were then cut into smaller chunks followed by passing it through a blender to form uniform shredded dried bacterial cellulose. To maintain the particle consistency, the grounded cellulose sheets were sieved in order to consider particles which measured 300 μm. To maintain the same concentration of both the sources derived hydrogel, the measurements of TEMPO oxidation procedure were kept the same. Briefly, 0.5 g of dried 300 μm cellulose powder was added to 50 ml of water. Then TEMPO (8 mg, 0.2 mmol) and NaBr (51.2 mg, 2 mmol) were added to the cellulose powder water mix followed by NaOCl solution (5% w/v, 20 mmol) in a dropwise manner. pH was maintained at 10.5 and regulated by 0.5 M NaOH until no more variation was observed. After the reaction was completed the oxidized cellulose fibers were washed for a few times until the pH dropped to 7.4. The fibers were then homogenized using an ultrasonic probe homogenizer (Fisherbrand™ Model 505) to get a final concentration of 1% (w/v) CNF hydrogel.

4.4. Rheological characterization

TA instrument, HR-2 Discovery Hybrid Rheometer equipped with Environmental Test Chamber, USA was used to determine the rheological characterization of the formulated cellulose hydrogels. The best ideal suited test geometry was a 20 mm diameter plate. Both the formulated hydrogels P-CNF and B-CNF were placed below the Peltier plate and the shaft was lowered to maintain a working distance of 1900 mm. The excess hydrogel was always discarded after lowering the shaft and then the measurements were performed in a sequential pattern. The tests were performed in triplicates to represent the average and the standard deviation. The stiffness of various prepared cellulose hydrogel samples was monitored for calculating the storage modulus with applied 2% strain, 100–0.1 rad/s angular frequency and at temperature recorded at 23 °C. The shear viscosity (η) of both hydrogel systems was also recorded at different shear rates ranging from 0.01 to 1000 s^{-1}.

4.5. FTIR

Fourier transform infrared (FTIR) spectra of pure raw cellulose and dried CNF hydrogel (both TOPC and TOBC) were obtained using an FTIR spectrometer (VERTEX 70 FTIR, Bruker Optik GmbH, Germany) with a resolution of 4 cm^{-1} and accumulation of 1866 scans between 4000 and 400 cm^{-1} on ATR mode.

4.6. Scanning electron microscopy

The formulated CNF hydrogels were examined post preparation and also after extrusion from the 3D printer for the fiber morphology, porosity and cell distribution. The CNF gel samples were prepared using critical point drying post sequential treatment in gradient ethanol solution. The dehydrated samples were then analyzed using SEM (JEOL JSM-7600F, Japan) at 10 Kv accelerating voltage. The dried samples were gold coated for 40 s before imaging.

4.7. Swelling test

The printed scaffolds were first weighed in the wet state (post overnight incubation in media) after removing the excess media with a pipette. Constructs were then dried in a freeze dryer for about 20–30 min after chilling them at − 80 ℃ for about 20 min. The dried scaffolds were weighed then immersed in media again. After 5 min, 30 min, 2 h, 5 h and 24 h the scaffolds were weighed to calculate the reabsorption capability.

4.8. Degradation assay

To determine the degradation profile of the 3D printed CNF hydrogel scaffolds with varying infill density in the presence of cellulase enzyme derived from *Trichoderma reesei* (Sigma-Aldrich, Missouri, USA), the printed moulds were submerged in a bath of cellulase enzyme post

prolonged overnight incubation in cell culture medium. The enzyme concentration was maintained at (150 μg/mg). For diluting the enzyme cell culture medium was used to support the encapsulated cells while the degradation process was going on. After the enzyme was added to the printed scaffolds with varying infill density, the incubation was carried out at 37 ºC, 5% CO_2. After every 5 h the degraded cellulose was discarded and the remaining solid mass was weighed. Then fresh enzyme solution was again added to continue the reaction till the point the entire 3D printed mould was completely degraded. The experiment was carried out in triplicates to obtain the mean and the standard deviation.

4.9. Cell culture

Mouse embryonic stem cells R1/E was purchased from ATCC, USA. The conditioned media used for the study consisted of DMEM (Thermo Fisher Scientific), 1% Sodium Pyruvate (Thermo Fisher Scientific, USA), 15% FBS (Gibco, USA), 1X non-essential amino acids (Thermo Fisher Scientific, USA), 1% L-Glutamax (Thermo Fisher Scientific, USA), 0.1 mM 2-ß Mercaptoethanol (Thermo Fisher Scientific, USA), 1% Penicillin-Streptomycin(Nacalai Tesque, Japan) and 1000 U/ml Leukemia Inhibiting Factor (LIF) (was added prior to use) (Life Technologies, Thermo Fisher, USA) to maintain the pluripotency. The cell culture flask was treated with gelatin (0.1%) (Sigma Aldrich, USA) before seeding the cells. The cells were monitored until 60% confluency before Trypsin-EDTA (0.25%) (Nacalai Tesque, Japan) dissociation. The growth medium was switched every alternate day to make sure the cells were healthy and alive. The cell maintenance was performed at 37 °C and 5% CO_2. The cell line was used at passage 10 for carrying out the cell encapsulation study. Similarly, we also chose to use NIH-3T3 cell line purchased from ATCC, USA. The growth medium used for maintaining this cell was the basis medium which consisted of DMEM (Nacalai Tesque, Japan), 10% FBS (Gibco, USA) and 1% Penicillin-Streptomycin (Nacalai Tesque, Japan). The cells were maintained in cell culture flask with changing media every 2–3 days and upon 80% confluency the cells were Trypsin-EDTA (0.25%) dissociated and used for the cell encapsulation study. We used passage number 20 for NIH-3T3 cell line.

4.10. 3D cell encapsulation

For carrying out the cell encapsulation and viability assay, mouse embryonic stem cells (R1/E) and mouse fibroblasts cells (NIH-3T3) were used. The cells were trypsin dissociated followed by encapsulating them thoroughly in TOPC and TOBC. Briefly, the dissociated cells around 3×10^7 cells/ml was mixed slowly into the CNF hydrogel of both types. Then the hydrogels were aliquoted into the syringe barrel which would later be installed onto the printer for printing the scaffolds. Cell encapsulated gels were incubated in presence of cell culture medium at 37 °C, 5% CO_2. The samples were studied in triplicate with continuous replacement of medium every 24 h. On Day 1,5, 7 and 10 the CNF hydrogels were checked to study the cell viability before and after degrading the scaffold. Post degradation of the scaffolds the cells were washed thoroughly to ensure removal of all the left out residual enzymes. Confocal microscopy was performed on the cell laden hydrogels to understand the 3D distribution of the cells and the cell morphology. The hydrogels with cells were excited at 488/543 nm and images were captured in the form of z-stacks at an interval of 20 μm.

4.11. Direct bioink writing

3D printing was performed using a pneumatic-based direct ink writing (DIW) printer (SHOTmini 200Sx, Musashi Engineering, Inc., Tokyo Japan). The printing process was conducted in an enclosed chamber to maintain a sterile condition. The designs of the mesh structures of different infills (12.5%, 18%, 25%, 50% and 100%) were designed using MuCAD V (Musashi Engineering, Inc., Tokyo, Japan). The mass of all prints was kept constant at 0.2 g. All formulated cellulose gels were loaded into a luer-lock dispensing syringe fitted with 20 G (Birmingham Gauge) nozzle. The syringe was then placed onto the syringe holder on the DIW printer. The substrates used in this work were cover slits with the dimension of 22 mm by 22 mm. The printing speed and dispensing pressure were also calibrated according to the viscosity of the gels. All printings were conducted at room temperature.

4.12. Cell recovery analysis

The cell recovery was studied by degrading the hydrogel using cellulase hydrogel and counting the total number of cell released. An automated cell counter (Thermo Fisher Scientific) was used to determine the values. The number generally includes both live and the dead cell density. This gives an estimate and comparison between the initial number of cell encapsulated and the number of cell released by the end of the experiment.

4.13. Cell viability assay

To check the viability of the encapsulated cells LIVE/DEAD viability/cytotoxicity assay kit (Invitrogen, Thermo Fisher Scientific) was used. The prepared dye was added to the CNF hydrogel encapsulated cells and incubated for 15 min in the dark at 37 °C. Post incubation the gels were washed with 1X PBS to remove the excess dye and then the printed parts were imaged in a confocal microscope (Carl Zeiss, LSM-710 Germany). The green fluorescent images indicated live cells and red depicted dead cells.

4.14. Flow cytometry

The cell encapsulated bioinks post printing were incubated for 10 days. On day 1, 5, 7 and 10 the constructs were degraded with cellulase enzyme, the released cells were fixed with 4% paraformaldehyde for 15 min followed by permeabilization with 0.1% Triton X-100 (Nacalai Tesque,Japan). Then they were incubated with 5% BSA for blocking the cells before incubating with primary antibody. Blocking was carried out for 60 min at room temperature. Then the BSA treated cells were incubated overnight at 4 °C with anti OCT-4 (1:200) (Life Technologies, Thermo Fisher). The following day, cells were incubated with secondary antibody conjugated Alexa Fluor 488 (1:500) (Life Technologies, Thermo Fisher) for 60 min at room temperature. At last DAPI (4', 6-diamidino-2-phenylindole-2HCl (1:1000) (Life Technologies, Thermo Fisher)) was added and incubated for 5 min. Note, after each step there was a step of 1X PBS wash for 5 min each (3 washes). The cells were finally re-suspended in the 1X-PBS before running it through the flow cytometry machine (MACSQuantify).

4.15. Gene expression analysis

RNA from the extracted cells was obtained using the RNeasy Micro Kit (QIAGEN). Total DNA was retro-transcribed from the obtained RNA using a High Capacity Complementary DNA Reverse-Transcription kit (Thermo Fisher Scientific). Gene expression was determined by quantitative real time PCR on a Biorad(CFX Connect Real-Time PCR detection system) using SYBR green master mix (Thermo Fisher Scientific). Individual gene expression normalization was performed with respect to GAPDH.

4.16. Statistical analysis

Comparison between all the sets of data groups was performed using a Student's *t*-test. All the results here is represented as mean ± standard error (S.E.M). The significance is defined at $p < 0.05$.

Funding sources

This work was partially supported by the National Research Foundation, Singapore (grant number: CRP20-2017-0004).

Author statement

R.D. and J.G.F. conceived the idea and designed the experiments. R. D. performed the experiments, and collected and analyzed the data. A.P. established the culture and production of bacteria cellulose. C.P.L and M.H. assisted with the 3D printing of the scaffolds. R.D. and J.G.F. wrote the manuscript, with input of all the other authors.

Declaration of Competing Interest

The authors declare that they have no known competing financial interests or personal relationships that could have appeared to influence the work reported in this paper.

Acknowledgments

The authors would like to thank Cellulose Lab (Canada) for providing free samples of cellulose slurry to carry out our preliminary experiments. Also, we would like to thank the MIT-SUTD International Design Center (IDC) and the SUTD Digital Manufacturing and Design Centre (DManD) in Singapore for the use of their equipment and installations.

Appendix A. Supporting information

Supplementary data associated with this article can be found in the online version at doi:10.1016/j.mtcomm.2021.103023.

References

[1] R. Naomi, R. Bt Hj Idrus, M.B. Fauzi, Plant-vs. bacterial-derived cellulose for wound healing: a review, Int. J. Environ. Res. Public Health 17 (18) (2020) 6803.
[2] R. Das, J.G. Fernandez, Cellulose nanofibers for encapsulation and pluripotency preservation in the early development of embryonic stem cells, Biomacromolecules (2020).
[3] M. Sponchioni, C. O'Brien, C. Borchers, E. Wang, M. Rivolta, N. Penfold, I. Canton, S. Armes, Probing the mechanism for hydrogel-based stasis induction in human pluripotent stem cells: is the chemical functionality of the hydrogel important? Chem. Sci. 11 (1) (2020) 232–240.
[4] B. Baghaei, M. Skrifvars, All-cellulose composites: a review of recent studies on structure, properties and applications, Molecules 25 (12) (2020) 2836.
[5] M. Szymańska-Chargot, M. Chylińska, K. Gdula, A. Kozioł, A. Zdunek, Isolation and characterization of cellulose from different fruit and vegetable pomaces, Polymers 9 (10) (2017) 495.
[6] K. Radotić, M. Mićić, Methods for extraction and purification of lignin and cellulose from plant tissues. Sample Preparation Techniques for Soil, Plant, and Animal Samples, in: Springer, Springer, 2016, pp. 365–376.
[7] S.D. Dutta, D.K. Patel, K.-T. Lim, Functional cellulose-based hydrogels as extracellular matrices for tissue engineering, J. Biol. Eng. 13 (1) (2019) 55.
[8] C. Xu, B.Z. Molino, X. Wang, F. Cheng, W. Xu, P. Molino, M. Bacher, D. Su, T. Rosenau, S. Willför, 3D printing of nanocellulose hydrogel scaffolds with tunable mechanical strength towards wound healing application, J. Mater. Chem. B 6 (43) (2018) 7066–7075.
[9] Y. Wu, Z.Y.W. Lin, A.C. Wenger, K.C. Tam, X.S. Tang, 3D bioprinting of liver-mimetic construct with alginate/cellulose nanocrystal hybrid bioink, Bioprinting 9 (2018) 1–6.
[10] K. Markstedt, A. Mantas, I. Tournier, H.C. Martínez Ávila, D. Hagg, P. Gatenholm, 3D bioprinting human chondrocytes with nanocellulose–alginate bioink for cartilage tissue engineering applications, Biomacromolecules 16 (5) (2015) 1489–1496.
[11] T. Tronser, A. Laromaine, A. Roig, P.A. Levkin, Bacterial cellulose promotes long-term stemness of mesc, ACS Appl. Mater. Interfaces 10 (19) (2018) 16260–16269.
[12] I. Canton, N.J. Warren, A. Chahal, K. Amps, A. Wood, R. Weightman, E. Wang, H. Moore, S.P. Armes, Mucin-inspired thermoresponsive synthetic hydrogels induce stasis in human pluripotent stem cells and human embryos, ACS Cent. Sci. 2 (2) (2016) 65–74.
[13] Y.-R. Lou, L. Kanninen, T. Kuisma, J. Niklander, L.A. Noon, D. Burks, A. Urtti, M. Yliperttula, The use of nanofibrillar cellulose hydrogel as a flexible three-dimensional model to culture human pluripotent stem cells, Stem Cells Dev. 23 (4) (2014) 380–392.
[14] U.-J. Kim, N. Isobe, S. Kimura, S. Kuga, M. Wada, J.-H. Ko, H.-O. Jin, Enzymatic degradation of oxidized cellulose hydrogels, Polym. Degrad. Stab. 95 (12) (2010) 2277–2280.
[15] R. Bardet, J. Bras, Cellulose nanofibers and their use in paper industry. Handbook of Green Materials: 1 Bionanomaterials: Separation Processes, Characterization and Properties, World Scientific, 2014, pp. 207–232.
[16] F. Esa, S.M. Tasirin, N. Abd Rahman, Overview of bacterial cellulose production and application, Agric. Agric. Sci. Procedia 2 (2014) 113–119.
[17] L.J. Gibson, The hierarchical structure and mechanics of plant materials, J. R. Soc. Interface 9 (76) (2012) 2749–2766.
[18] Y. Huang, C. Zhu, J. Yang, Y. Nie, C. Chen, D. Sun, Recent advances in bacterial cellulose, Cellulose 21 (1) (2014) 1–30.
[19] A. Rashad, K. Mustafa, E.B. Heggset, K. Syverud, Cytocompatibility of wood-derived cellulose nanofibril hydrogels with different surface chemistry, Biomacromolecules 18 (4) (2017) 1238–1248.
[20] C.-N. Wu, S.-C. Fuh, S.-P. Lin, Y.-Y. Lin, H.-Y. Chen, J.-M. Liu, K.-C. Cheng, TEMPO-oxidized bacterial cellulose pellicle with silver nanoparticles for wound dressing, Biomacromolecules 19 (2) (2018) 544–554.
[21] J. Wei, Y. Chen, H. Liu, C. Du, H. Yu, J. Ru, Z. Zhou, Effect of surface charge content in the TEMPO-oxidized cellulose nanofibers on morphologies and properties of poly (N-isopropylacrylamide)-based composite hydrogels, Ind. Crops Prod. 92 (2016) 227–235.
[22] M. Bhattacharya, M.M. Malinen, P. Lauren, Y.-R. Lou, S.W. Kuisma, L. Kanninen, M. Lille, A. Corlu, C. GuGuen-Guillouzo, O. Ikkala, Nanofibrillar cellulose hydrogel promotes three-dimensional liver cell culture, J. Control. Release 164 (3) (2012) 291–298.
[23] D. McCune, X. Guo, T. Shi, S. Stealey, R. Antrobus, M. Kaltchev, J. Chen, S. Kumpaty, X. Hua, W. Ren, Electrospinning pectin-based nanofibers: a parametric and cross-linker study, Appl. Nanosci. 8 (1–2) (2018) 33–40.
[24] T. Saito, A. Isogai, TEMPO-mediated oxidation of native cellulose. The effect of oxidation conditions on chemical and crystal structures of the water-insoluble fractions, Biomacromolecules 5 (5) (2004) 1983–1989.
[25] H. Azeredo, H. Barud, C.S. Farinas, V.M. Vasconcellos, A.M. Claro, Bacterial cellulose as a raw material for food and food packaging applications, Front. Sustain. Food Syst. 3 (2019) 7.
[26] H. Yan, X. Chen, H. Song, J. Li, Y. Feng, Z. Shi, X. Wang, Q. Lin, Synthesis of bacterial cellulose and bacterial cellulose nanocrystals for their applications in the stabilization of olive oil pickering emulsion, Food Hydrocoll. 72 (2017) 127–135.
[27] C. Reynolds, R. Thompson, T. McLeish, Pressure and shear rate dependence of the viscosity and stress relaxation of polymer melts, J. Rheol. 62 (2) (2018) 631–642.
[28] T. Yeung, P.C. Georges, L.A. Flanagan, B. Marg, M. Ortiz, M. Funaki, N. Zahir, W. Ming, V. Weaver, P.A. Janmey, Effects of substrate stiffness on cell morphology, cytoskeletal structure, and adhesion, Cell Motil. Cytoskelet. 60 (1) (2005) 24–34.
[29] M. Gharpuray, Y.H. Lee, L. Fan, Structural modification of lignocellulosics by pretreatments to enhance enzymatic hydrolysis, Biotechnol. Bioeng. 25 (1) (1983) 157–172.
[30] X. Chen, Degradation Studies on Plant Cellulose and Bacterial Cellulose by FT-IR and ESEM, University of Birmingham, 2015.
[31] H. Grethlein, D. Allen, A. Converse, A comparative study of the enzymatic hydrolysis of acid-pretreated white pine and mixed hardwood, Biotechnol. Bioeng. 26 (12) (1984) 1498–1505.
[32] H.E. Grethlein, The effect of pore size distribution on the rate of enzymatic hydrolysis of cellulosic substrates, Bio/Technology 3 (2) (1985) 155–160.
[33] A. Fiorati, N. Contessi Negrini, E. Baschenis, L. Altomare, S. Faré, A. Giacometti Schieroni, D. Piovani, R. Mendichi, M. Ferro, F. Castiglione, A. Mele, C. Punta, L. Melone, TEMPO-nanocellulose/Ca2+ hydrogels: ibuprofen drug diffusion and in vitro cytocompatibility, Materials 13 (1) (2020) 183.
[34] N.D. Sanandiya, J. Vasudevan, R. Das, C.T. Lim, J.G. Fernandez, Stimuli-responsive injectable cellulose thixogel for cell encapsulation, Int. J. Biol. Macromol. 130 (2019) 1009–1017.
[35] J.G. Fernandez, S. Seetharam, C. Ding, J. Feliz, E. Doherty, D.E. Ingber, Direct bonding of chitosan biomaterials to tissues using transglutaminase for surgical repair or device implantation, Tissue Eng. Part A 23 (3–4) (2016) 135–142.
[36] X. Hu, Z. Yang, S. Kang, M. Jiang, Z. Zhou, J. Gou, D. Hui, J. He, Cellulose hydrogel skeleton by extrusion 3D printing of solution, Nanotechnol. Rev. 9 (1) (2020) 345–353.
[37] C. Xie, Q. Gao, P. Wang, L. Shao, H. Yuan, J. Fu, W. Chen, Y. He, Structure-induced cell growth by 3D printing of heterogeneous scaffolds with ultrafine fibers, Mater. Des. 181 (2019), 108092.
[38] A. Suurnäkki, M. Tenkanen, M. Siika-aho, M.-L. Niku-Paavola, L. Viikari, J. Buchert, Trichoderma reesei cellulases and their core domains in the hydrolysis and modification of chemical pulp, Cellulose 7 (2) (2000) 189–209.
[39] M. Tenkanen, J. Puls, K. Poutanen, Two major xylanases of Trichoderma reesei, Enzym. Microb. Technol. 14 (7) (1992) 566–574.